communications earth & environment

ARTICLE

https://doi.org/10.1038/s43247-023-00937-9 OPEN

Weak influence of the secondary surface processes on the regolith of Chang'E-5 landing site

Junjie Li[1✉], Ziying Li[1✉], Zhixin Huang[1], Ting Li[1], Dongfa Guo[1], Hanbin Liu[1], Guang Fan[1], Mingkuan Qin[1], Liang Lei[2], Xin Zhou[3], Hailong Wang[4], Kaiyu Wang[2], Xiangbo Gao[2], Apeng Yu[1], Ruiping Liu[1], Jia Zhang[1], Liumin Deng[1], Sheng He[1], Yong Wu[1] & Linfei Qiu[1]

Noble gases in lunar soils provide critical information regarding solar wind and cosmic-ray interactions with the lunar surface, as well as the history of impact events affecting the regolith turnover processes. Here, we studied the characteristics of noble gases He, Ne, Ar in Chang'E-5 soil. High $^{4}He/^{36}Ar$ and $^{20}Ne/^{36}Ar$ values show that the soil has typical mare terrain characteristics. Furthermore, both values are higher than those in other lunar soils, suggesting the secondary processes occurring in the soil may have been less strong than in other lunar samples. Trapped $(^{3}He/^{4}He)_{tr}$ and $(^{20}Ne/^{22}Ne)_{tr}$ values were less fractionated than those of Apollo soils, also indicating the weak secondary processes the Chang'E-5 soil underwent. Trapped $(^{40}Ar/^{36}Ar)_{tr}$ values indicate the implanted solar wind was young. The integrated exposure times to solar wind of the soil on the lunar surface suggest the Chang'E-5 soil was not seriously admixed by sputtered material from nearby rocks.

[1] Beijing Research Institute of Uranium Geology, Beijing 100029, China. [2] Westlake University, Hangzhou 310024, China. [3] National Institute of Measurement and Testing Technology, Chengdu 610021, China. [4] China Academy of Engineering Physics, Mianyang 621900, China. ✉email: 564484480@163.com; zyli9818@126.com

Noble gases in lunar soils are mainly sourced from solar wind implantation, in situ decay of radionuclides (notably radiogenic $^{4}He_{r}$ and $^{40}Ar_{r}$ from the decay of U and Th and ^{40}K, respectively), and spallation of the target nuclides irradiated by cosmic rays (for instance, cosmogenic $^{3}He_{c}$, $^{21}Ne_{c}$, and $^{38}Ar_{c}$). They provide a critical record of the evolution of the sun and the complex physical processes that have occurred on the lunar surface[1–5]. The results of previous noble gas analyses of samples from the Apollo and Luna missions showed obvious variations, which were closely related to lunar soil origin, the frequency and intensity of impact events, and the interaction of the solar wind with the lunar surface[1,6,7].

China's Chang'E-5 mission successfully returned 1731 g of lunar soil from the Northern Oceanus Procellarum of the Moon on December 17, 2020. The landing site is located at a relatively high latitude which has not been previously reached and far from the Apollo and Luna landing sites. The site was selected because of the presence of young basaltic rocks as deduced by impact crater counting. The age of the rocks was later confirmed by the precise Pb–Pb dating, with a crystallization age of 1963 ± 57 Ma reported by Che et al.[8] and 2030 ± 4 Ma reported by Li et al.[9]. The returned soil is among the youngest maria on the moon found so far[8–10]. In this study, we report on the concentrations and isotopic compositions of He, Ne, and Ar of the Chang'E-5 lunar soil (hereafter, CE-5 soil) to better understand the related physical processes that occurred on the new landing site over the past 2 Ga years.

Results and discussion

The Chang'E-5 sample studied in this work was a fine-grained soil sample scooped from the lunar surface (Sample number: CE5C0100YJFM001). The grains included mineral fragments, basaltic clasts, agglutinates, breccias, and glasses (Fig. 1), and the grain size was concentrated in the range of 1–200 μm[11]. We conducted He, Ne, and Ar analyses on the bulk soil, different grain sizes fractions, and different types of minerals (ilmenite, plagioclase, and pyroxene-olivine) and glass beads. In addition, single grains or groups of a few mineral grains were selected for Micro-CT scanning. In that process, the surface area and volume of each grain were measured in order to examine the correlation of noble gas concentration with the surface area and volume of the grains.

Elemental abundance ratios. The concentrations of all three noble gases (He, Ne, and Ar) in the soil showed a significant negative correlation with the grain size (Supplementary Data 1). The smaller the grain size, the larger the specific surface area. Thus, the concentrations of noble gases in CE-5 soil have an obvious positive correlation with the surface area. As previously reported, the implantation depth of the solar wind ions is only several tens of nanometers, which renders the solar wind gas concentration closely dependent on the grain surface area[12–14]. Therefore, the strong surface-correlation of the noble gas concentrations in the CE-5 soils suggests that the noble gases are sourced predominantly from the implantation of solar wind. The most recent measurement of unfractionated elemental ratios and isotopic compositions of solar wind He, Ne, and Ar were carried out by Heber et al. with targets from the Genesis mission (Table 1)[15]. However, it is inevitable that the solar wind noble gases trapped in lunar soils become fractionated. The extent of fractionation is not only closely related to the secondary processes (e.g., micrometeorite impacts, soil transportation and burial, and the irradiation of cosmic rays) that occurred on the lunar soils but also to the different retentivity of noble gases in different minerals in the soil.

Signer et al. reported that the specific retention efficiency of different minerals for He and Ne is quite different (retention efficiency: ilmenite > olivine-pyroxene > plagioclase), while all minerals retain solar wind Ar similarly well[16]. This was now also observed in the CE-5 soil we studied, as the ^{36}Ar concentrations of all three minerals were essentially the same, differing by only ~7%. Conversely, the ^{4}He and ^{20}Ne concentrations of different minerals exhibited obvious differences. Expectedly, the ilmenite has the highest $^{4}He/^{36}Ar$ and $^{20}Ne/^{36}Ar$ values, demonstrating its best He and Ne retentivity. In contrast, the plagioclase with the lowest $^{4}He/^{36}Ar$ and $^{20}Ne/^{36}Ar$ ratios revealed large losses of He and Ne. However, the very similar $^{4}He/^{36}Ar$ values in both the plagioclase and pyroxene-olivine groups demonstrated that the latter group also had poor He retentivity. In comparison, the higher $^{20}Ne/^{36}Ar$ value of pyroxene-olivine indicated that it could better retain Ne than plagioclase (Fig. 2). The glass beads group has even lower concentrations of three noble gases than all three mineral types, possibly due to part of the glass beads having been formed from solar wind bearing particles by impact events that resulted in severe losses of these gases.

The elemental ratios of $^{4}He/^{36}Ar$ and $^{20}Ne/^{36}Ar$ could be used to distinguish the origin of the lunar soil, as material from mare terrains is significantly richer in He and Ne than that from highland regions, mainly because the mare soils are richer in ilmenite than highland soils[7,16]. Signer et al. summarized the $^{4}He/^{36}Ar$ and $^{20}Ne/^{36}Ar$ values of the soils from highland and mare samples. The $^{4}He/^{36}Ar$ and $^{20}Ne/^{36}Ar$ values of the soils from the highland are seldom higher than 150 and 3, respectively, whereas those of soils from mare are significantly higher, exceeding 200 and 4, respectively[16]. For the CE-5 soils analyzed in this study, the mean $^{4}He/^{36}Ar$ and $^{20}Ne/^{36}Ar$ ratios are 661.1 and 7.1, respectively (Fig. 3 and Supplementary Data 1), clearly showing

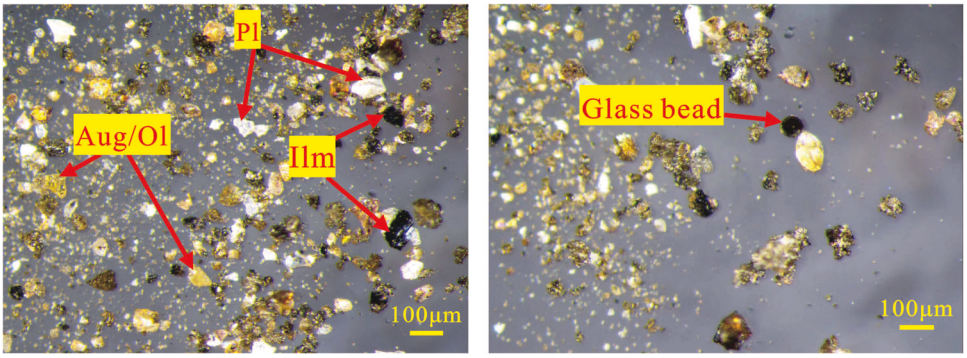

Fig. 1 Images of the bulk sample under the microscope. Ilm ilmenite: black, opaque, euhedral, or subhedral crystals; Pl plagioclase: colorless to white, transparent, euhedral, or subhedral crystals; Aug/Ol pyroxene-olivine: yellow to light brown, transparent, euhedral, or subhedral crystals; Glass beads: round beads with variable colors and uniform transparency.

Table 1 Elemental and isotopic composition of He, Ne, and Ar of solar wind collected by the Genesis mission[15].

Elemental compositions		Isotopic compositions			
$\frac{^4He}{^{20}Ne}$	$\frac{^{20}Ne}{^{36}Ar}$	$\frac{^3He}{^4He}$	$\frac{^{20}Ne}{^{22}Ne}$	$\frac{^{21}Ne}{^{22}Ne}$	$^{38}Ar/^{36}Ar$
656 ± 5	42.1 ± 0.3	(4.64 ± 0.09) × 10^{-4}	13.78 ± 0.03	0.0329 ± 0.0001	0.1828 ± 0.0003

Uncertainty of each value is 1σ.

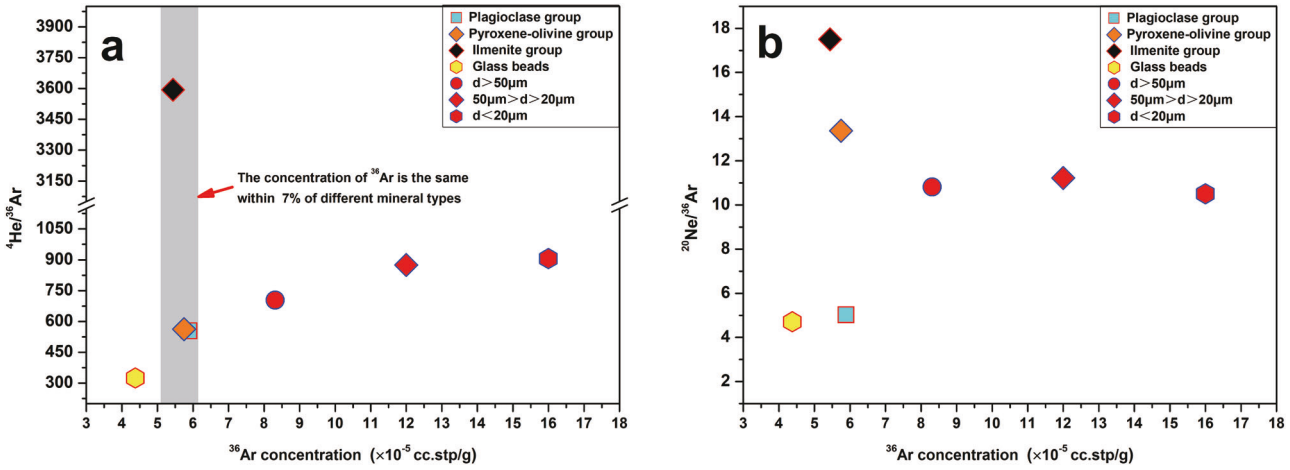

Fig. 2 Elemental ratios of different minerals and soil with different grain sizes versus their ^{36}Ar concentrations. a ^{4}He/^{36}Ar ratios plotted versus ^{36}Ar concentrations. **b** ^{20}Ne/^{36}Ar ratios plotted versus ^{36}Ar concentrations.The uncertainties (1σ) of the data are smaller than symbol sizes.

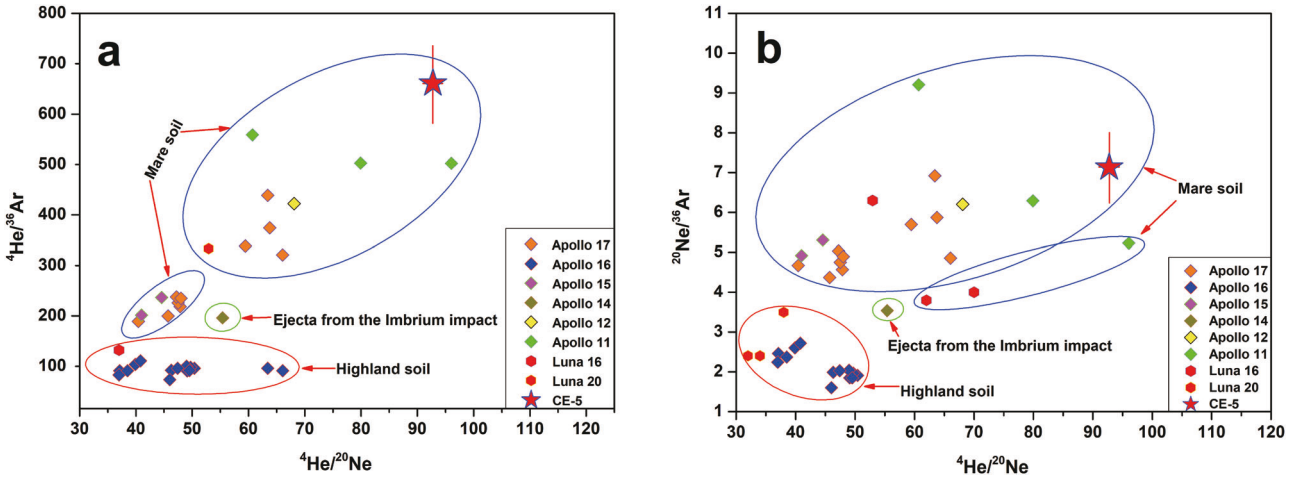

Fig. 3 Elemental abundance ratios of the different lunar soils. a ^{4}He/^{36}Ar ratios plotted versus ^{4}He/^{20}Ne ratios. **b** ^{20}Ne/^{36}Ar ratios plotted versus ^{4}He/^{20}Ne ratios.Unfractionated solar wind ^{4}He/^{36}Ar and ^{20}Ne/^{36}Ar ratios were shown in Table 1. It could be seen that ^{4}He/^{36}Ar ratio and ^{20}Ne/^{36}Ar ratios in mare soils are less fractionated than those in highland soils. Furthermore, CE-5 soils seem to preserve more light noble gas compared with most mare soils returned by other missions. Analytical uncertainties of ^{4}He/^{36}Ar ratio and ^{20}Ne/^{36}Ar ratio of CE-5 soil are at 1σ. The elemental abundance ratios of Apollo and Luna soils are from refs. [7,16–19,27,50–56].

that the soil has typical mare terrain characteristics. In addition, the ^{4}He/^{36}Ar and ^{20}Ne/^{36}Ar values obtained in this study were higher than those of most mare soils from the Apollo and Luna missions. It is reported that the Ti-rich samples appear to have better He and Ne retentivity; hence, they tend to have higher ^{4}He/^{36}Ar and ^{20}Ne/^{36}Ar ratios relative to Ti-poor samples[7,17–21]. Taking the TiO_2 content into consideration, we compared the ^{4}He/^{36}Ar and ^{20}Ne/^{36}Ar ratios of the CE-5 soil with those of the soil samples retrieved by Apollo and Luna missions. To avoid the grain size effect, the data we used for the comparison were generally from samples with approximately the same grain size. Even considering the effect of the TiO_2 content of the local basalt, both the ^{4}He/^{36}Ar and ^{20}Ne/^{36}Ar ratios of CE-5 lunar soil show relatively high values (Fig. 4), indicating that the solar wind in CE-5 soil was less fractionated than that in most other lunar soils. The high ^{4}He/^{36}Ar and ^{20}Ne/^{36}Ar values of CE-5 soil indicate that the soil suffered only relatively weak secondary processes. Such processes could be caused by a variety of factors, including micrometeorite impacts, cosmic rays irradiation, soil burial and compaction, mixing with hot ejecta from craters, and so on. They could lead to surface erosion of the soil grains, which in turn result in the partial loss of solar wind gas from the soil. It is natural to recognize that the lighter noble gas (e.g., He) is more sensitive to such secondary

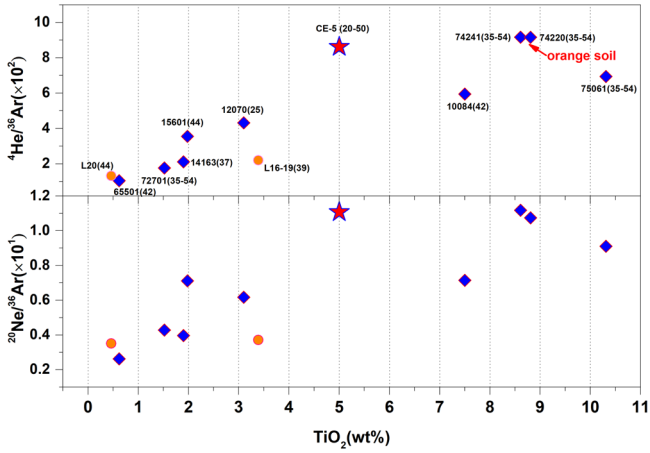

Fig. 4 Relationship between TiO_2 contents and $^4He/^{36}Ar$ and $^{20}Ne/^{36}Ar$ ratios of the lunar soils. The number in the brackets indicates the soil grain size(the unit of the grain size is μm). The data of the Apollo and the Luna soils are from ref. [17,50–56].

processes than the heavier noble gas (e.g., Ar). Therefore, the weaker these secondary processes are, the higher the $^4He/^{36}Ar$ and $^{20}Ne/^{36}Ar$ values of the soil are likely to be. Thus, the high $^4He/^{36}Ar$ and $^{20}Ne/^{36}Ar$ values of CE-5 soil may indicate that the secondary processes it endured were not strong.

Isotopic compositions. The measured values of $(^3He/^4He)_m$ of the bulk sample ranged from $(3.91 \pm 0.06) \times 10^{-4}$ to $(4.18 \pm 0.06) \times 10^{-4}$ [mean value: $(4.02 \pm 0.11) \times 10^{-4}$], $(^{20}Ne/^{22}Ne)_m$ from 12.57 (±0.16) to 13.08 (±0.16) [mean value:12.88 (±0.22)], and $(^{21}Ne/^{22}Ne)_m$ from 0.038(±0.001) to 0.042 (±0.001)[mean value: 0.040 ± (0.002)] (Supplementary Data 1). The $^{20}Ne/^{22}Ne$ and $^{21}Ne/^{22}Ne$ values prove that the noble gas in CE-5 soil is solar wind dominated as they all plot in the area between the fractionated solar wind and solar wind in the neon three-isotope plot (Supplementary Fig. 2). The isotopic composition differences of the bulk samples may be a result of inhomogeneity due to the very small sample size for each analysis. The measured values do not accurately represent the trapped noble gas isotopic composition because the samples also contain a small fraction of in situ radiogenic (^4He_r) and cosmogenic nuclides (^3He_c,$^{20}Ne_c$, $^{21}Ne_c$, and $^{22}Ne_c$) that should be properly subtracted. The grain size dependence of the $(^3He/^4He)_m$ and $(^{21}Ne/^{22}Ne)_m$ ratios allows for calculating the concentrations of the volume correlated ^3He_c and $^{21}Ne_c$[17,19,22]. For example, one could plot the $(^{21}Ne/^{22}Ne)_m$ versus $1/^{21}Ne_m$ of different grain size fractions to calculate the $(^{21}Ne/^{22}Ne)_{tr}$ from the ordinate intercept of the line and $^{21}Ne_c$ from the slope of the least square fit. Unfortunately, however, our data did not show the correlation between the grain size and isotopic composition as described in the literature, mostly because we could not prepare well-defined homogeneous grain size fractions due to the very small sample size available (Supplementary Fig. 3). Therefore, we attempted to calculate the cosmic-ray exposure (CRE) age to evaluate the contribution of the cosmogenic nuclides ^3He_c, $^{20}Ne_c$, and $^{22}Ne_c$. In principle, ^3He_c,$^{21}Ne_c$, and $^{38}Ar_c$ all could be used to calculate the CRE age. However, the ^3He_c does not work because we couldn't correct the measured ^3He for the dominant solar wind $^3He_{sw}$.The $^{38}Ar_c$ is also difficult to calculate as the measured $(^{38}Ar/^{36}Ar)_m$ value (Supplementary Data 1) is too close to the solar wind $(^{38}Ar/^{36}Ar)_{sw}$ value (Table 1), which means that the amount of $^{38}Ar_c$ is too small compared with the solar wind $^{38}Ar_{sw}$. In contrast, the $(^{21}Ne/^{22}Ne)_m$ values are different enough from the solar wind value to reliably calculate $^{21}Ne_c$. Assuming $(^{21}Ne/^{22}Ne)_{tr} = 0.03125$ (±0.00101) and $(^{21}Ne/^{22}Ne)_c = 0.91$ (±0.08) reported by Signer et al.[16], we calculated the $^{21}Ne_c$ exposure age by adopting the production rates reported by Leya et al.[23] for 2π irradiation geometry. Since these are related to the soil depth, here we adopted the maximum production rate assuming the depth of the sample during irradiation near the lunar surface was 30 g/cm^2. The exposure ages of bulk samples calculated in this way ranged from 363 (±45) to 566 (±86) Ma, with an average age of 432 (±116) Ma (Supplementary Data 2). As discussed above, such variable $^{21}Ne_c$ exposure ages of the bulk soil also result from the inhomogeneity of the samples due to the extremely small sample size we used. What should be noted here is that, as discussed above, considerable Ne loss occurred due to diffusion; therefore, the ^{21}Ne exposure ages should be regarded as a lower limit to the true exposure time to cosmic rays radiation. Based on the $^{21}Ne_c$ values, the ^3He_c concentration of the soils was calculated according to the production rate given by Reedy[24]. However, a large fraction of ^3He_c may have been lost via diffusion on the lunar surface[25,26]. We were unable to clarify this loss as it is closely related to the exposure history of the soil, and the physical processes that occurred on the soil like the flux and intensity of the micrometeorite impacts. Somewhat arbitrarily assuming a 50% loss of ^3He_c by diffusion, the retained ^3He_c amount would account for 4.8–7.7% of the amount of measured ^3He in CE-5 soil. As for the radiogenic ^4He_r, we calculated its concentration through the U and Th contents reported by Li et al.[11] and the rock age of ~2 Ga determined by Pb–Pb dating[8,9].Also adopting a 50% loss of ^4He_r, the retained ^4He_r fraction would not exceed 1% of the measured ^4He. With these corrections, the trapped $(^3He/^4He)_{tr}$ ratios of the bulk samples range between$(3.73 \pm 0.06) \times 10^{-4}$ and $(3.89 \pm 0.06) \times 10^{-4}$, which seem similar to values reported for Apollo 11 and Apollo 15 soils[17,27,28]. The isotopic compositions of He and Ne of different minerals also exhibited significant variations. The $(^3He/^4He)_m$ value in the pyroxene-olivine group was relatively high [$(4.66 \pm 0.08) \times 10^{-4}$)], whereas, in the ilmenite and plagioclase groups, the $(^3He/^4He)_m$ values were relatively low [$(4.13 \pm 0.06) \times 10^{-4}$) and $(4.12 \pm 0.06) \times 10^{-4}$), respectively]. The glass beads group had the lowest $(^3He/^4He)_m$ value, indicating that severe fractionation occurred during the mineral remelting process to form the beads. We consider that the $(^3He/^4He)_m$ value of the pyroxene-olivine group may have been significantly higher than that in the ilmenite group due to a relatively large contribution of the cosmogenic nuclide ^3He_c. Assuming that the ilmenite and olivine-pyroxene groups had the same exposure age, we adopted a mean exposure time of bulk soils with 432 Ma (Supplementary Data 2) to estimate the concentrations of the ^3He_c in different mineral groups according to their different production rates (Supplementary Data 3).The calculated concentration of ^3He_c in the pyroxene-olivine group was only slightly higher than that in the ilmenite group because-unlike for $^{21}Ne_c$ and $^{38}Ar_c$-elemental production rates of ^3He_c only weakly depend on the chemical composition of a mineral. Therefore, the slight difference in ^3He_c concentration between these two mineral groups would be insufficient to result in a significant difference in their $(^3He/^4He)_m$ values, as long as the concentrations of trapped He in both samples would be comparable. However, as discussed above, the concentration of solar wind $^3He_{sw}$ trapped in ilmenite was significantly higher than that in pyroxene-olivine, leading to a lower proportion of ^3He_c to $^3He_{sw}$ in ilmenite relative to that of pyroxene-olivine. In other words, the contribution of ^3He_c in pyroxene-olivine must be obviously higher than that in ilmenite. This must be the dominant reason for the higher $(^3He/^4He)_m$ value of the pyroxene-olivine group. After the ^3He_c subtraction (also assuming a 50% loss of diffusion), we obtained $(^3He/^4He)_{tr}$

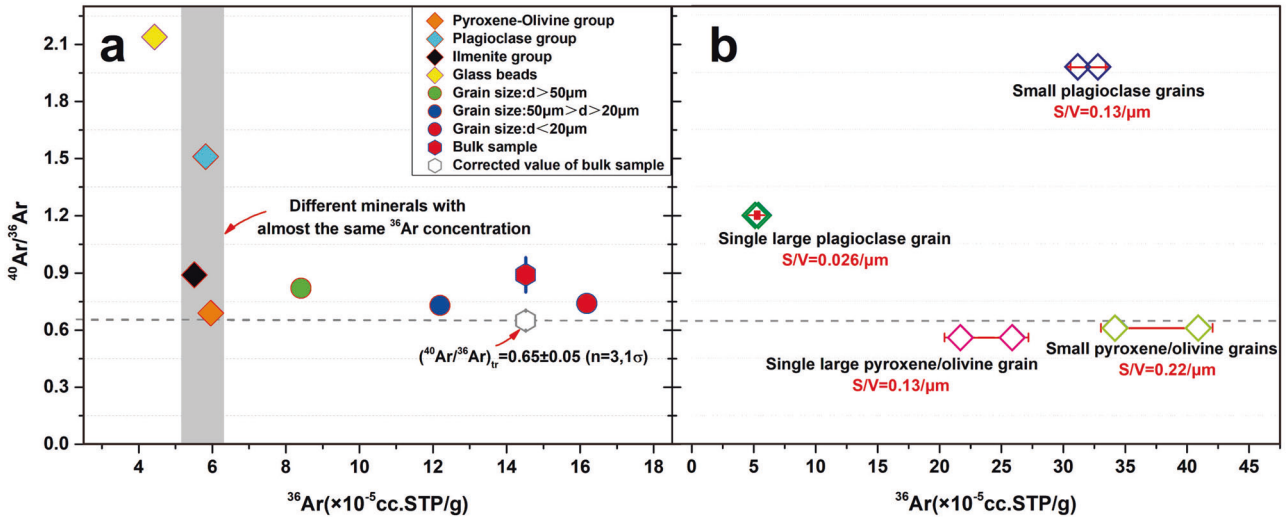

Fig. 5 $(^{40}Ar/^{36}Ar)_m$ ratios plotted versus the ^{36}Ar concentrations in CE-5 soil. a $(^{40}Ar/^{36}Ar)_m$ ratios in different minerals and soil with different grain sizes. Different minerals have similar ^{36}Ar concentrations, and the grain size negatively correlates with the ^{36}Ar concentration. **b** $(^{40}Ar/^{36}Ar)_m$ ratios in groups with single (several) grain(s). Note that each group has two symbols representing the grain weight, which is related to the ^{36}Ar concentration and is calculated by the two end-densities of the mineral, respectively. The $^{40}Ar/^{36}Ar$ ratios of the single (several) pyroxene/olivine grain(s) are close to the corrected $(^{40}Ar/^{36}Ar)_{tr}$ ratios of the bulk soil, as they have negligible radiogenic ^{40}Ar because of the extremely low *K* content. Analytical uncertainties of the $^{40}Ar/^{36}Ar$ ratio of the bulk sample are at 1σ. The uncertainties of the ^{36}Ar concentration of the single (several) pyroxene/olivine grain(s) mainly resulted from the uncertainty of the mineral density and uncertainty of grain volume determination (see details in the "Methods" section).

values of $(4.07 \pm 0.06) \times 10^{-4}$ for the ilmenite group and $(4.17 \pm 0.07) \times 10^{-4}$ for the pyroxene-olivine group, showing that the $(^3He/^4He)_{tr}$ values of the two groups were more similar than the $(^3He/^4He)_m$ values. To obtain the $(^{20}Ne/^{22}Ne)_{tr}$ value, we subtracted $^{22}Ne_c$ according to the $(^{21}Ne/^{22}Ne)_c = 0.91$ (±0.08)[16], the corrected $(^{20}Ne/^{22}Ne)_{tr}$ values of the bulk samples ranged from 12.71 (±0.16) to 13.17 (±0.16). The ilmenite group, which exhibited the best Ne retentivity, showed a higher $(^{20}Ne/^{22}Ne)_{tr}$ value of 13.64 (±0.17) relative to other mineral groups (Supplementary Data 4). The relatively low value in the glass beads group, as in the case of $(^3He/^4He)_{tr}$, indicates a pronounced isotopic mass fractionation effect due to the significant gas loss during the melting process.

The trapped $(^{40}Ar/^{36}Ar)_{tr}$ value is a semi-quantitative measure of the solar wind antiquity of lunar soils[20,29–33]. As the solar wind is essentially free of ^{40}Ar, the trapped ^{40}Ar in the soil is basically entirely derived from the lunar exosphere by ionization and acceleration by the electromagnetic field induced by the solar wind and final implantation into the soil, while the trapped ^{36}Ar derives from the solar wind. The ^{40}Ar in the exosphere, which is mainly sourced from the radioactive decay of the ^{40}K in the lunar interior, has decreased over time[30–32]. Therefore, the smaller $(^{40}Ar/^{36}Ar)_{tr}$ values are, the younger the solar wind and the soils preserved. Eugster et al. reported that the $(^{40}Ar/^{36}Ar)_{tr}$ values decrease from about 13 some 3.7 Ga ago, to about 0.5 for samples irradiated during the last several 10 Ma ago[31]. For CE-5 soil, the most reliable $(^{40}Ar/^{36}Ar)_{tr}$ may come from the potassium-poor pyroxene-olivine group because the contribution of radiogenic $^{40}Ar^*$ produced by the ^{40}K decay process is very small. The pyroxene-olivine group had a $(^{40}Ar/^{36}Ar)_m$ value of 0.69 (±0.01). The single pyroxene-olivine grain returned a $(^{40}Ar/^{36}Ar)_m$ value of 0.56 (±0.01), which must be very close to the trapped $(^{40}Ar/^{36}Ar)_{tr}$ value of the CE-5 soil, as the contribution of the radiogenic ^{40}Ar was negligible. Therefore, the CE-5 soil was likely irradiated relatively late in lunar history, perhaps as late as 10 Ma ago, but certainly later than 1 Ga ago. The relatively higher $(^{40}Ar/^{36}Ar)_m$ value of the pyroxene-olivine group compared to that of the pyroxene-olivine single grain may have resulted from K-bearing impurities in the pyroxene-olivine group (Supplementary Data 5). The glass beads and plagioclase mineral groups showed relatively higher $(^{40}Ar/^{36}Ar)_m$ values relative to the pyroxene-olivine group, which must be due to the radiogenic $^{40}Ar_r$ contribution of the samples. Higher $(^{40}Ar/^{36}Ar)_m$ values were also found in the two single (several) plagioclase grain(s) groups. Regarding the difference in the $^{40}Ar/^{36}Ar$ values of these two groups, we believe it may result from the inhomogeneity in K between the different grains. The average $(^{40}Ar/^{36}Ar)_m$ value of the analyzed CE-5 bulk soil was 0.87 (±0.09) (Supplementary Data 1). After subtraction of radiogenic $^{40}Ar_r$ calculated through the K contents reported by Li et al.[11] and the rock age of ~2 Ga determined by Pb–Pb dating[8,9], we corrected the $(^{40}Ar/^{36}Ar)_{tr}$ of the bulk sample with the value of 0.65 (±0.05) that was expectedly consistent with the $(^{40}Ar/^{36}Ar)_{tr}$ value of the pyroxene-olivine group, which is free of the contribution of radiogenic $^{40}Ar^*$ (Fig. 5).

The $(^3He/^4He)_{tr}$ ratio inversely correlates with the $(^{40}Ar/^{36}Ar)_{tr}$ value (Fig. 6). As discussed above, the lower the $(^{40}Ar/^{36}Ar)_{tr}$ value, the more recent the solar wind captured by the soil. Based on this, it has been argued that the $^3He/^4He$ of the solar wind may have increased over time[34,35]. This apparent secular change in $(^3He/^4He)_{sw}$ was explained by the mixing of the ^3He produced by the incomplete burning of H in the outer convective zone of the sun, which is the solar wind source[36,37]. However, Heber et al. measured $(^3He/^4He)_{tr}$ using the high-resolution closed system stepwise etching method, which could effectively extract the solar wind He and Ne through the precise control of the erosion depth of the soils[38–41], and found that not only the apparent solar wind $(^3He/^4He)_{sw}$ increases with the antiquity of the solar wind, but the $(^{20}Ne/^{22}Ne)_{sw}$ appears to show a similar increase[41]. The magnitude of the increase in $^{20}Ne/^{22}Ne$ was ~5%/Ga, which is difficult to explain. Therefore, it is suggested that the apparent increase in $(^3He/^4He)_{tr}$ of the soils with young antiquity age may be caused by secondary processes of the soils on the lunar surface[2,39–41]. As discussed above, the secondary processes could result in the partial removal of the solar wind component that resides at the outmost layer of

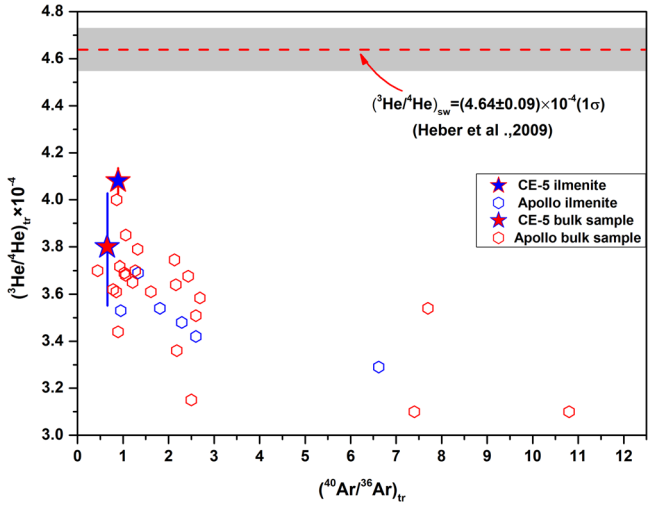

Fig. 6 Correlation of the $(^3He/^4He)_{tr}$ ratios versus $(^{40}Ar/^{36}Ar)_{tr}$ ratios of the lunar samples. The latter is an antiquity indicator of the solar wind, as introduced above. The $(^3He/^4He)_{tr}$ ratios of the CE-5 bulk soil and ilmenite both fit the correlation. The uncertainties of $(^3He/^4He)_{tr}$ ratios of CE-5 samples were estimated on the assumption that the cosmogenic ^3He and radiogenic ^4He with different loss proportions (the symbol represents 50% loss of ^3He_c). The data of Apollo soils are from previous reports[16,17,19,22,28,31,53,54,57].

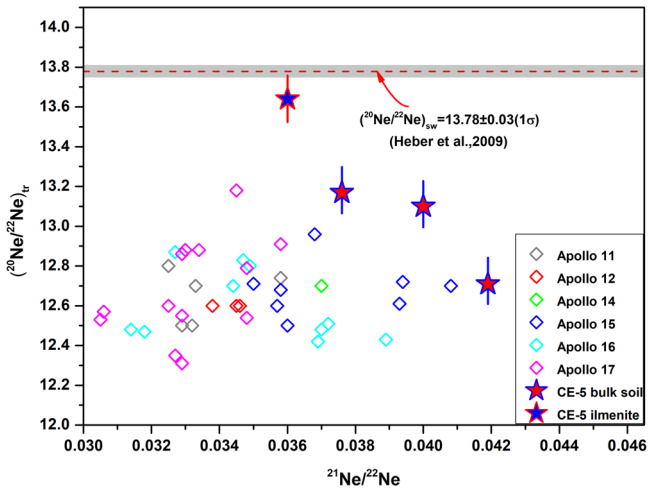

Fig. 7 Comparison of the isotopic composition of Ne in the lunar soil. The $(^{20}Ne/^{22}Ne)_{tr}$ ratios of the CE-5 bulk soil seem less fractionated than those of the Apollo soils, particularly for the $(^{20}Ne/^{22}Ne)_{tr}$ ratio in ilmenite, which is very close to that of the modern solar wind, indicating that the secondary process endured by the CE-5 soils was not strong. The relatively higher $^{21}Ne/^{22}Ne$ ratios of the CE-5 soil than those of other lunar soils indicate that the sample contains a certain proportion of cosmogenic ^{21}Ne, which may result from the longer cosmic-ray irradiation time than those of the Apollo samples. The uncertainties of $(^{20}Ne/^{22}Ne)_{tr}$ ratios in CE-5 samples are at 1σ. The data of Apollo soils are from previous reports[16,17,19,22,28,31,53,54,57].

the grains. It was shown that the trapped solar noble gases become isotopically heavier in the deeper grain layers[41]. Thus, the stronger the secondary processes the soil endured, the more severe the isotopic fractionation of the trapped solar wind noble gas was. We compared the $(^3He/^4He)_{tr}$ and $(^{20}Ne/^{22}Ne)_{tr}$ values in CE-5 soils with those in other lunar soils (Figs. 6 and 7). Both the $(^3He/^4He)_{tr}$ and $(^{20}Ne/^{22}Ne)_{tr}$ values of the CE-5 soil are less fractionated than in other lunar soils, i.e. the CE-5 values plot closer to the unfractionated solar wind values. Especially the ilmenite, shows a $(^{20}Ne/^{22}Ne)_{tr}$ ratio very close to that of the unfractionated solar wind, probably the least fractionated value reported for a lunar soil so far. This remarkable finding indicated that the secondary processes the CE-5 soils have undergone were weak. This observation is in agreement with the relatively good retention of solar wind ^4He and ^{20}Ne, indicated by the relatively high $^4He/^{36}Ar$ and $^{20}Ne/^{36}Ar$, which also indicated that the trapped noble gas record in the CE-5 soil is less disturbed by secondary processes than that of other lunar soils. As discussed above, multiple reasons could lead to such secondary processes. Further work is required to better understand the fractionation processes in detail, but the CE-5 soil seems to be indeed a particularly valid extension to the lunar sample suite.

Integrated exposure time. The integrated exposure time refers to the time that the soil is directly exposed to the solar wind on the uppermost lunar surface[16]. We used the concentration of ^{36}Ar, which is better retained than ^4He and ^{20}Ne, to estimate the integrated exposure time of the soil. Geiss et al. measured the solar wind flux using a metallic foil at the lunar surface and obtained a ^{36}Ar flux of the solar wind of 600 atoms cm^{-2} s^{-1}[42,43], based on which the effective acquisition rate of the outermost regolith layer could be calculated as ~1.1×10^{-10} cm^3 · STP cm^{-2} yr^{-1}[16]. Therefore, if the surface area and the ^{36}Ar amount could be measured for each mineral grain, it would be possible to estimate the integrated mean residence time of the grain in the uppermost layer of the regolith. Signer et al. calculated the integrated exposed times of the Apollo minerals with 150–200 μm grain size, ~2000 (soil 60051) to 13,000 years (soil 15021)[16]. We conducted Micro-CT scanning for each grain of four groups (two groups with single grain and the other two groups with several grains) to determine the surface area of each group, after which the grains of each group were totally melted to determine the ^{36}Ar amount. The results showed that the ^{36}Ar amounts of all four groups are linearly correlated with their surface areas, and the ^{36}Ar amount per grain surface area in all four groups was similar (Fig. 8, Supplementary Data 6). These findings indicate that the grains of each group may have endured the same exposure-burial history. According to the implanted rate of the ^{36}Ar mentioned above, we calculated the integrated exposure times of the four groups to be between 4778 (±57)and 6168 (±189) years on the assumption that no ^{36}Ar was lost. Compared with the Apollo soils, it appeared that the integrated exposure time of CE-5 soil was in the middle range. However, considering that the basalt of the Chang'E-5 landing site is relatively young (~2 Ga) compared to that of the Apollo landing site (3.0–4.5 Ga), and assuming that the CE-5 soil is derived from the local basalt, the integrated exposure time of the minerals of CE-5 must be close to the upper limit of those of the Apollo soils if the turnover frequency of the lunar sample is constant during the lunar history. Signer et al. suggested that the relatively short integrated exposure time of the sample may indicate that the soil was admixed by grains sputtered from the impact of nearby rocks, as the grains formed by the impact of the rocks may not have been previously exposed to the solar wind[16]. From this point, the relatively long integrated exposure time of the CE-5 minerals may indicate that the soil of the CE-5 landing site was not admixed by sputtered materials from nearby rocks seriously.

Methods

Sample preparation. Sample preparation work was carried out in an ultra-clean room to avoid contamination of the surroundings. Firstly, three aliquots sample with very small amounts (sample weight: ~0.1 mg of each aliquot) were taken from the sample bottle, then transferred to three small copper cups (wall thickness: 0.15 mm, inner

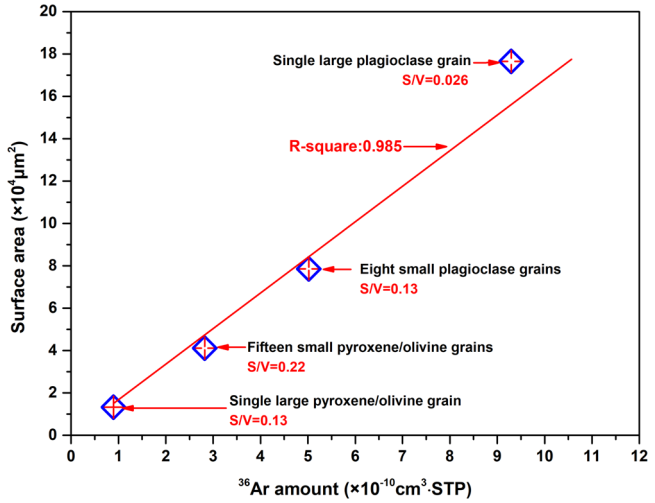

Fig. 8 ^{36}Ar amount of the grain(s) plotted versus its(their) surface area. S/V represents the ratio of surface area to volume of the grain(s). The ^{36}Ar amount correlates well with the surface area but shows no relationship with the volume.

diameter: 4 mm, height: 5 mm) (Supplementary Fig. 1). A sample in each copper cup was completely melted in one step by the laser for He, Ne, and Ar analyses.

Secondly, another two aliquots (sample weight: ~1 mg for each aliquot) were taken from the vials for mineral separation and grain size sorting, respectively. According to their different colors and shapes, three mineral groups with >80% of target minerals (ilmenite, pyroxene-olivine, and plagioclase) and one group with 100% glass beads were identified. Three additional groups of different grain sizes were selected (då 50 μm, 50 μmå då 20 μm, and d <20 μm) according to the length of the longest side of the grain from another aliquot of the CE-5 bulk sample. Both the mineral separation and grain size selection were carried out under a binocular microscope using hand-picking method. Except for the glass beads group, each group was randomly divided into two portions. One portion was cast in epoxy resin as standard 25-mm mounts for mineral identification and grain size analysis. The other portion was transferred to a small copper cup (Supplementary Fig. 1), which was used to weigh the sample mass by a precise balance and then also as a crucible placed into the laser chamber for the noble gas extraction. No statistical work on mineralogy was conducted on glass beads due to the extremely small amount.

Lastly, four additional groups of minerals with single or several grains were selected from the CE-5 bulk soil, two groups being plagioclase grains and two olivine-pyroxene grains. One plagioclase group consisted of a single large grain (grain size: ~200 μm), while the other represented several small grains (grain sizes: 50–100 μm). Similarly, one of the olivine-pyroxene groups consisted of one single grain (grain size: ~200 μm) and the other group included several smaller grains (grain sizes: 50–100 μm). All grains were adhered to glue tape for Micro-CT scanning to measure the surface area and volume. After scanning, the mineral grains were removed from the tape and transferred to the copper cup for gas extraction by laser melting method.

Mineral and grain size characterization. The quantitative mineral analysis and particle size statistics of each group in this study were determined using a Zeiss Sigma 300 scanning electron microscope, equipped with a Bruker X Flash 6130 energy dispersive spectrometer with an advanced mineral identification and characterization system. It operated at 15 kV, and a resolution of 0.11–0.93 μm/pixel. The maximum length calculation method was used to determine the particle size, and the particle size distribution were calculated by the weight of the particles in different size range as a percentage of the total weight of all particles. For the estimate of the bulk soil composition, modal abundances of the different mineral and glass phases were converted to mass abundance using the following densities:2.73 g/cm^3 for anorthite, 3.40 g/cm^3 for clinopyroxene, 3.7 g/cm^3 for olivine, 4.39 g/cm^3 for fayalite, 3.24 g/cm^3 for glass, 4.72 g/cm^3 for ilmenite, 4.78 g/cm^3 for ulvöspinel, 4.75 g/cm^3 for troilite, 2.62 g/cm^3 for silica, 3.15 g/cm^3 for apatite, 5.75 g/cm^3 for baddeleyite, 4.79 g/cm^3 for chromite, 7.6 g/cm^3 for iron, 4.65 g/cm^3 for zircon, and 2.52 g/cm^3 for K-bearing minerals. On this basis, accurate identification of minerals was carried out using electron probe data. The chemical composition of different lunar minerals and glass was determined by wavelength dispersive spectroscopy using a JXA-8100 electron microprobe operating at 20 kV, 10 nA, with a 1–2 μm beam diameter.

Measurement of the surface area and volume of single grain. This study used an Xradia 610 Versa micro-CT scanner to obtain the surface area and volume of the mineral (plagioclase, pyroxene, and olivine) grains. The voltage of the X-ray source was 120 kV and the 20 X detector was applied to obtain a voxel size as fine as 0.25 μm. Such a small voxel size guarantees that even the smallest particle is represented by at least thousands of voxels to depict the particle morphology. This study used a machine-learning algorithm "ilastik" (the official website ilastik.org provides further details) to conduct mineral segmentation from raw CT images that considers both voxel intensity and mineral edge detection at the same time[44].

The volume of each particle was then obtained by counting the voxel number of a particle with known unit voxel volume. 3D erode (peels off a layer of voxels from the 3D volume) and dilate (adds a layer of voxels to the 3D volume) functions in Fiji were utilized to estimate the surface area of the particles[45]. The surface area of each particle was determined by dividing the total volume of eroded and dilated voxels by the thickness of the surface layer. We consider the maximum uncertainty in volume calculation to occur when the whole surface layer was mistakenly classified, therefore, the uncertainty value was calculated by dividing the eroded or dilated voxels over the total volume. The number of voxels in the eroded surface layer is typically slightly less than the dilated counterpart, and the difference between the number of eroded and dilated voxels divided by their average was considered as the uncertainty in particle surface area calculation. The image intensity is correlated to the mineral composition and density[46,47]. Minerals with higher density and higher average atomic number are brighter in CT images. Sometimes, the boundary between different minerals is not sharp and there could be a gradual transition between different minerals, and even a single mineral grain could show variation in image brightness as its composition may change gradually. Through image segmentation, we could determine the number of mineral types in a single grain, to check whether the particle was pure or not. The plagioclase grains are obviously dark due to relatively low density and low average atomic number. However, it is more difficult to clearly distinguish between pyroxene and olivine due to their similar density. Even under the binocular, these two minerals show the same yellow color. Therefore, we put pyroxene and olivine into one group for discussion.

He, Ne, and Ar analyses

Sample weighing. To minimize sample loss, for weighing we transferred the sample directly to the copper cup in which the sample was later melted. We first weighed the empty crucible on a high-precision balance (resolution:0.001 mg), then added the sample and weighed the crucible with the sample. Each sample was weighed four times to ensure the accuracy of the weights. For single grains or assemblages of a few grains, this method would not have been precise enough, therefore, the sample masses were calculated by the volume of the grain determined by Micro-CT, and the respective mineral density. The uncertainty of the weight determination of these samples was mainly governed by the uncertainty of the mineral density. For the pyroxene-olivine minerals, it was difficult to separate the pyroxene and olivine under the microscope; hence, we used the densities of 3.40 g/cm^3 for pyroxene and 4.07 g/cm^3 for olivine to determine the mass uncertainty. For plagioclase, we used a density between 2.56 g/cm^3 and 2.69 g/cm^3.

Gas extraction. A CO_2 laser ($\lambda = 10.6$ μm) was used to extract the gas by total-fusion. A small copper cup containing the weighed sample was placed into a copper holder in the laser chamber. After evacuating the chamber to high vacuum, it was baked at 100 °C for 72 h to fully remove the adsorbed atmospheric gas. Finally, the sample was melted with a 2-mm-diameter laser beam and ~8 W of power. After each extraction, the power was increased to 10 W to check that the sample gas had been thoroughly extracted upon melting.

Gas analysis. The extracted noble gases were purified using three SAES ST-101 getters, two getters at 450 °C and another one at room temperature. He, Ne, and Ar were analyzed using a Helix SFT (Thermo Fisher Scientific) split flight tube noble gas mass spectrometer in static mode. After purification, the heavier noble gases (Ar, Kr, and Xe) were trapped by a charcoal finger immersed in liquid nitrogen, leaving the pure He and Ne to be let into the mass spectrometer for analysis. The two He isotopes were simultaneously measured (^{4}He on the Faraday cup and ^{3}He on the multiplier). The three Ne isotopes were detected in peak-jumping mode (^{20}Ne and ^{22}Ne on the Faraday cup and ^{21}Ne on the multiplier). A charcoal finger at 77 K near the ion source was used to freeze the Ar and CO_2 during measurements. Even so, the $^{40}Ar^+$ and CO_2^+ were measured during each analysis for correction of interferences of the $^{40}Ar^{++}$ and CO_2^{++} to the ^{20}Ne and ^{22}Ne. However, the $^{40}Ar^+$ signal was seldom beyond 1% of the ^{20}Ne signal; thus, the contribution of $^{40}Ar^{++}$ to $^{20}Ne^+$ was negligible. The CO_2^+ signal was not more than 10% of that of $^{22}Ne^+$. Considering the correction factor of the CO_2^{++}/CO_2^+ (1.3 ± 0.3%)[48], the contribution of the CO_2^{++} to $^{22}Ne^+$ was ~0.1%, thus it could also be neglected. After the He and Ne analysis, the charcoal finger was heated to release the heavier noble gases for the Ar analysis. The three Ar isotopes were also measured in peak-jumping mode (^{40}Ar and ^{36}Ar on the Faraday cup and ^{38}Ar on the multiplier).

Data correction. The standard for the correction of the measured ^{3}He/^{4}He value of lunar soil was an artificial gas mixture with a ^{3}He/^{4}He value of ~5.00E−04, more than two orders of magnitude higher than the atmospheric value of ~1.40E-06.To ascertain its accurate He isotopic composition, the standard gas was distributed to several associated laboratories at ETH (Zurich, Switzerland), INGV (Palermo, Italy), and IGGCAS (Beijing, China) for comparison. The ^{3}He/^{4}He ratios of the three laboratories closely agree with each other (Supplementary Data 7) and we adopt the

average value of $4.95(\pm0.07)\times10^{-4}$. The Ne and Ar isotopic compositions were corrected for mass discrimination with an air standard. The He and Ne concentrations of the samples were calculated by comparing the corresponding signal intensity with those of known amounts of the air standard. Ar concentrations of the samples were calibrated with the ^{40}Ar-^{39}Ar dating sanidine standard YBCs. Splits of this standard, with a radiogenic $^{40}Ar^{*}$ abundance of $1.16(\pm0.01)\times10^{-5}$cc·STP/g(calculated by its K content and crystallization age proposed by Wang et al.[49]), were precisely weighed and then melted to release $^{40}Ar^{*}$.

The blanks were measured according to the same procedure used for the sample analysis. For the laser method, the mean blank levels were $1.01(\pm0.05)\times10^{-10}$ cc. STP in ^{4}He, $1.98(\pm0.08)\times10^{-12}$ cc. STP in ^{20}Ne, and $3.59(\pm0.09)\times10^{-11}$ cc. STP in ^{40}Ar with the laser turned off. All blanks were measured before individual sample analysis and subtracted for sample correction.

Data availability

All data tables were uploaded to an open-source repository at https://doi.org/10.5281/zenodo.7986711. The data are also available in the supplementary information.

Received: 21 November 2022; Accepted: 19 July 2023;
Published online: 02 August 2023

References

1. Bogard, D. D., Funkhouser, J. G., Schaeffer, O. A. & Zähringer, J. Noble gas abundances in lunar material-cosmic ray spallation products and radiation ages from the sea of tranquility and the ocean of storms. *Geophys. Res. Lett.* **76**, 2757–2779 (1971).
2. Wieler, R. & Heber, V. S. Noble gas isotopes on the moon. *Space. Sci. Rev.* **106**, 197–210 (2003).
3. He, H. Y., Wang, Y. & Deng, C. Noble gases in the lunar soil. *Geochimica* **39**, 123–130 (2010).
4. Curran, N. Unravelling the history of the lunar regolith. Doctoral thesis. The University of Manchester. 1–175 (2017).
5. Curran, N. et al. A database of noble gases in lunar samples in preparation for mass spectrometry on the Moon. *Planet. Space. Sci.* **182**, https://doi.org/10.1016/j.pss.2019.104823 (2020).
6. Zou, Y. L., Xu, L. & Ouyang, Z. Y. Noble gases in the lunar regolith. *Geochimica* **22**, 361–368 (2003).
7. Walton, J. R., Lakatos, S. & Heymann, D. Distribution of inert gases in fines from the Cayley-Descartes region. *Geochim. Cosmochim. Acta* **2**, 2079–2095 (1973).
8. Che, X. C. et al. Age and composition of young basalts on the Moon, measured from samples returned by Chang'e-5. *Science* **374**, 887–890 (2021).
9. Li, Q. L. et al. Two-billion-year-old volcanism on the Moon from Chang'E-5 basalts. *Nature* https://doi.org/10.1038/s41586-021-04100-2 (2021).
10. Qiao, L. et al. Geology of the Chang'E-5 landing site: constraints on the sources of samples returned from a young nearside mare. *Icarus* **364**, https://doi.org/10.1016/j.icarus.2021.114480 (2021).
11. Li, C. L. et al. Characteristics of the lunar samples returned by the Chang'E-5 mission. *Natl. Sci. Rev.* **9**, 16–28 (2022).
12. Wieler, R., Baur, H. & Signer, P. Noble gases from solar energetic particles revealed by closed system stepwise etching of lunar soil minerals. *Geochim. Cosmochim. Acta* **50**, 1997–2017 (1986).
13. Ozima, M. et al. Terrestrial nitrogen and noble gases in lunar soils. *Nature* **436**, 655–659 (2005).
14. Grimberg, A. et al. Solar wind neon from Genisis:Implication of the lunar noble gas record. *Science* **314**, 1133–1135 (2006).
15. Heber, V. S. et al. Noble gas composition of the solar wind as collected by the Genesis mission. *Geochim. Cosmochim. Acta* **73**, 7414–7432 (2009).
16. Signer, P. et al. Helium, neon, and argon records of lunar soil evolution. *In*: 8th Proc. Lunar Sci. Conf., 3657–3683 (1977).
17. Eberhardt, P., Geiss, J., Graf, H., Groegler, N. & Stettler, A. Trapped solar wind noble gases, exposure age and K/Ar-age in Apollo 11 lunar fine material. *Science* **167**, 558–560 (1970).
18. Heymann, D., Yaniv, A. & Lakatos, S. Inert gases in twelve particles and one "dust" sample from Luna 16. *Earth Planet. Sci. Lett.* **13**, 400–406 (1972).
19. Hintenberger, H., Weber, H. W. & Schultz, L. Z. Solar, spallogenic, and radiogenic rare gases in Apollo 17 soils and breccias. *Geochim. Cosmochim. Acta* **2**, 2005–2022 (1974).
20. Kirsten, T., Steinbrunn, F. & Zähringer, J. Location and variation of trapped rare gases in Apollo 12 lunar samples. *In: 2nd Proc. Lunar Sci. Conf.* **2**, 1651–1669 (1971).
21. Yaniv, A. & Heymann, D. Inert gases from Apollo 11 and Apollo 12 fines: reversals in the trends of relative element abundances. *Earth Planet. Sci. Lett.* **10**, 387–391 (1971).
22. Hintenberger, H., Schulz, L. & Weber, H. W. A comparison of noble gases in lunar fines and soil breccias: implication for the origin of soil breccias. *In: 6th Proc. Lunar Sci. Conf.* 2261–2270 (1975).
23. Leya, I., Neumann, S., Wieler, R. & Michel, R. The production of cosmogenic nuclides by galactic cosmic-ray particles for 2π exposure geometries. *Meteorit. Planet.Sci.* **36**, 1547–1561 (2001).
24. Reedy, R. C. Cosmic-ray stable nuclides: various production rates and their implications. *In: 12th Proc. Lunar Sci. Conf.* 1809–1823 (1981).
25. Hohenberg, C. M., Marti, K., Podosek, F. A., Reedy, R. C. & Shirck, J. R. Comparisons between observed and predicted cosmogenic noble gases in lunar samples. *In: 9th Proc. Lunar Planet. Sci. Conf.* 2311–2344 (1978).
26. Yaniv, A. & Kirsten, T. Isotopic ratios of rare gases and the role of nuclear reactions in solar flares(abstract). *In: 12th Proc. Lunar Planet. Sci. Conf.* 1224–1226 (1981).
27. Hintenberger, H. & Weber, H. W. Trapped rare gases in lunar fines and breccias. *In: 4th Proc. Lunar Sci. Conf., Geochim. Cosmochim. Acta* **2**, 2003–2019 (1973).
28. Apollo 15 preliminary examination team. The Apollo 15 lunar samples: a preliminary description. *Science* **175**, 363–375 (1972).
29. Eugster, O., Geiss, J. & Grögler, N. Dating of early regolith exposure and the evolution of trapped ^{40}Ar/^{36}Ar with time. *In: 14th Lunar and Planet. Sci. Conf.*, 177–178 (1983).
30. Eugster, O. & Polnau, E. Further data for the calibration of the antiquity indicator ^{40}Ar/^{36}Ar for lunar soil. *In: 28th Lunar and Planet. Sci. Conf.*, 341–342 (1997).
31. Eugster, O., Terribilini, D., Polnau, E. & Kramers, J. The antiquity indicator argon-40/argon-36 for lunar surface samples calibrated by uranium-235-xenon-136 dating. *Meteorit. Planet. Sci.* **36**, 1097–1115 (2001).
32. Joy, K. H., Kring, D. A., Bogard, D. D., McKay, D. S. & Zolensky, M. E. Re-examination of the formation ages of the Apollo 16 regolith breccias. *Geochim. Cosmochim. Acta* **75**, 7208–7225 (2011).
33. Manka, R. H. & Michel, F. C. Lunar atmosphere as a source of argon-40 and other lunar surface elements. *Science* **169**, 278–280 (1970).
34. Geiss, J. Solar wind composition and implications about the history of the solar system. *Int. Cosmic Ray Conf.* **13th**, 3375–3398 (1973).
35. Wieler, R. The solar noble gas record in lunar samples and meteorites. *Space Sci. Rev.* **85**, 303–314 (1998).
36. Geiss, J. Solar-wind composition and implications about the history of the solar system. *13th Int. Cosmic Ray Conf.* **5**, 3375–3398 (1974).
37. Gloeckler, G. & Geiss, J. Measurement of the abundance of Helium-3 in the Sun and in the local interstellar cloud with SWICS on Ulysses. *Space Sci. Rev.* **84**, 275–284 (1998).
38. Benkert, J. P., Baur, H., Signer, P. & Wieler, R. He, Ne, and Ar from the solar wind and solar energetic particles in lunar ilmenites and pyroxenes. *J. Geophys. Res. Planets* **98**, 13147–13162 (1993).
39. Heber, V. S. Ancient solar wind noble gases in lunar and meteorite archives and tests for modern solar wind collection with the GENESIS mission. *Doctor thesis*, https://doi.org/10.3929/ethz-a-004377513 (2002).
40. Heber, V. S., Baur, H. & Wieler, R. Is there evidence for a secular variation of helium isotopic composition in the solar wind? *Meteorit. Planet. Sci.* **36**, A76–A77 (2001).
41. Heber, V. S., Baur, H. & Wieler, R. Helium in lunar samples analyzed by high-resolution stepwise etching: implications for the temporal constancy of solar wind isotopic composition. *The Astrophys.J.* **597**, 602–614 (2003).
42. Geiss,J., Bühler, F., Cerutti, H., Eberhardt, P. & Filleux, C. Solar wind composition experiment. *Apollo 16 Prelim. Sci. Rep.* NASA SP-315, 14.1–14.10 (1972).
43. Geiss, J. et al. The Apollo SWC experiment: results, conclusions, consequences. *Space Sci. Rev.* **110**, 307–335 (2004).
44. Sommer, C., Straehle,C.,Köthe, U.& Hamprecht, F. A. Ilastik: interactive learning and segmentation toolkit. *In: 2011 IEEE International Symposium on Biomedical Imaging: From Nano to Macro*, 230–233 (2011).
45. Schindelin, J. et al. Fiji: an open-source platform for biological-image analysis. *Nat. Methods* **9**, 676–682 (2012).
46. Ketcham, R. A. & Carlson, W. D. Acquisition, optimization and interpretation of X-ray computed tomographic imagery: applications tothe geosciences.Comput. *Geosci* **27**, 381–400 (2001).
47. Lei, L., Seol, Y. & Jarvis, K. Pore-scale visualization of methane hydrate-bearing sediments with micro-CT. *Geophys. Res. Lett.* **45**, 5417–5426 (2018).
48. Li, J. J., Liu, H. B. & Zhang, J. Ne and Ar isotope analysis of samples with high abundance ratios of Ar/Ne and low abundance of Ne by MMS and QMS. *J. Anal. At. Spectrom.* **34**, 1205–1215 (2019).
49. Wang, F. et al. YBCs sanidine: a new standard for ^{40}Ar/^{39}Ar dating. *Chem. Geol.* **388**, 87–97 (2014).
50. Heymann, D., Yaniv, A. & Lakatos, S. Inert gases from Apollo 12, 14, and 15 fines. *Geochim. Cosmochim. Acta* **2**, 1857–1863 (1972).
51. Agrawal, J. K., Gopalan, K. & Rao, M. N. Solar wind and cosmogenic rare gases in lunar 16 and 20 soils and their correlation with cosmic ray produced fossil tracks in lunar samples. *Pramana* **3**, 176–185 (1974).

52. Heymann, D., Lakatos, S. & Walton, J. R. Inert gases in a terra sample: measurement in six grain-size fractions and two single particles from Luna 20. *Geochim. Cosmochim. Acta* **37**, 875–885 (1973).
53. Hintenberger, H., Schultz, L. & Weber, H. W. Rare gases in ilmenite and bulk samples of Apollo 17 soils and breccias. *6th Lunar and Planet. Sci. Conf.* 370–372 (1975).
54. Hintenberger, H., Weber, H. W. & Takaoka, N. Concentrations and isotopic abundances of the rare gases in lunar matter. *2nd Proc. Lunar Sci. Conf. Geochim. Cosmochim. Acta Suppl.* **2**, 1607–1626 (1971).
55. Vinogradov, A. P. Preliminary data on lunar ground brought to earth by automatic probe "Luna-16". *In: 2nd Proc. Lunar Sci. Conf. Geochim. Cosmochim. Acta Suppl.* **2**, 1967–1980 (1971).
56. Yaniv, A. & Heymann, D. Atmospheric ^{40}Ar in lunar fines. *In: 3rd Proc. Lunar Sci. Conf. Geochim. Cosmochim. Acta Suppl.* **3**, 1967–1980 (1972).
57. Eugster, O. et al. The cosmic-ray exposure history of shorty crater samples-the age of shorty crater. *In: 8th Proc. Lunar Sci. Conf.* 3059–3082 (1977).

Acknowledgements

Thanks to all the staff of CNSA for their outstanding work for the successful return of the lunar sample. We feel grateful to Andrea Luca Rizzo, Henner Busemann, and Fei Su for their comparison work on the He gas standard. We also thank Rainer Wieler, Sheng Xu, and Biying Chen for their insightful and constructive comments. We appreciated Ren Li for helping us take the high-quality pictures in this paper. This study was funded by the National Natural Science Foundation of China(41973051 and 42002044), the Research Program of the State Administration of Science, Technology, and Industry for National Defense (H2002).

Author contributions

Research design: J.J.L., Z.Y.L., Z.X.H., T.L., D.F.G., and M.K.Q. sample preparation: R.P.L., S.H., Y.W., and L.F.Q. Mineral selection and characterization: T.L., G.F., A.P.Y., and L.M.D. Micro-CT scanning: L.L., K.Y.W., and X.B.G. He standard preparation: X.Z. and H.L.W. Noble gas analysis: J.J.L., H.B.L., and J.Z. Writing: J.J.L., T.L., and L.L. All authors contributed to the revision of the manuscript.

Competing interests

The authors declare no competing interests.

Additional information

Supplementary information The online version contains supplementary material available at https://doi.org/10.1038/s43247-023-00937-9.

Correspondence and requests for materials should be addressed to Junjie Li or Ziying Li.

Peer review information *Communications Earth & Environment* thanks Rainer Weiler, Mark Nottingham, and the other, anonymous, reviewer(s) for their contribution to the peer review of this work. Primary Handling Editors: Claire Nichols, Joe Aslin, and Clare Davis.